frontiers | Frontiers in Environmental Science

TYPE Original Research
PUBLISHED 04 January 2023
DOI 10.3389/fenvs.2022.1028468

OPEN ACCESS

EDITED BY
Chaoyang Xue,
Laboratoire de physique et chimie de l'environnement et de l'Espace (LPC2E), France

REVIEWED BY
Qifan Liu,
University of Science and Technology of China, China
Li Zhou,
Sichuan University, China

*CORRESPONDENCE
Lingyan Wu,
wuly@cma.gov.cn
Junying Sun,
jysun@cma.gov.cn

SPECIALTY SECTION
This article was submitted to Atmosphere and Climate, a section of the journal Frontiers in Environmental Science

RECEIVED 26 August 2022
ACCEPTED 02 December 2022
PUBLISHED 04 January 2023

CITATION
Wang J, Wu L, Sun J, Zhang S and Zhong J (2023), Characteristics of $PM_{2.5}$ and secondary inorganic pollution formation during the heating season of 2021 in Beijing.
Front. Environ. Sci. 10:1028468.
doi: 10.3389/fenvs.2022.1028468

Characteristics of $PM_{2.5}$ and secondary inorganic pollution formation during the heating season of 2021 in Beijing

Jialing Wang[1], Lingyan Wu[1]*, Junying Sun[1]*, Sinan Zhang[1,2] and Junting Zhong[1]

[1]State Key Laboratory of Severe Weather & Key Laboratory of Atmospheric Chemistry of CMA, Chinese Academy of Meteorological Sciences, Beijing, China, [2]Shaanxi Meteorological Observatory, Xi'an, China

Water-soluble inorganic ions (WSIIs) were measured online in Beijing during the heating season of 2021, during which Beijing 2022 Olympic and Paralympic Winter Games were hosted. The characteristics of $PM_{2.5}$ and water-soluble inorganic ions were investigated in general, as well as during the clean period, polluted period, and Olympic and Paralympic Winter Games periods. It was found that most of the polluted episodes occurred under conditions of low wind speed, temperature inversion, and high relative humidity. The total mass concentration of water-soluble inorganic ions during the polluted period and the clean period accounted for 38.2% and 61.4% of the $PM_{2.5}$ mass concentration, respectively. Both the sulfur oxidation ratio (SOR) and nitrogen oxidation ratio (NOR) showed a strong relationship with relative humidity. During the polluted period, the concentrations of secondary aerosols such as sulfate, nitrate, and ammonium (SNA) increased significantly. Secondary transformation was enhanced compared with that in the clean period. A polluted process after a snowfall event was selected to explore the mechanism of sulfate and nitrate formation under high relative humidity. The results would be beneficial to understanding the causes of pollution and helping the government to formulate effective measures to control air pollution in winter.

KEYWORDS

$PM_{2.5}$, water-soluble inorganic ions, heating season, secondary transformation, sulfur oxidation ratio

1 Introduction

Fine particulate matter ($PM_{2.5}$, particles with an aerodynamic diameter of 2.5 μm or less) has a significant adverse impact on air quality, decreased visibility, global climate, and human health (Geng et al., 2021; Hu et al., 2021; Xu et al., 2022). In January 2013, a series of severe haze pollution episodes occurred in eastern China. The peak of $PM_{2.5}$ hourly average mass concentration in Beijing and its surrounding areas exceeded 500 μg/m^3 (Wang et al., 2013; Liu et al., 2015; Huang et al., 2016; Ren et al., 2021). Since then, the

Chinese government has taken many measures to improve air quality in the Beijing area. For example, stricter emission standards have been issued for coal power plants, industry, and road vehicles since 2013. Although air quality has improved overall and primary pollutants such as SO_2 have decreased significantly, however, $PM_{2.5}$ pollution still occurs frequently, especially in winter (Elser et al., 2016; Wang et al., 2019b; Lachatre et al., 2019; Cao et al., 2021; Huang et al., 2021; Li et al., 2021; Dong et al., 2022).

At present, the formation mechanism of haze pollution dominated by $PM_{2.5}$ is still unclear (Xie et al., 2022), which has become one of the difficulties in air pollution control in Beijing. Many researchers have explored the causes of $PM_{2.5}$ from different perspectives (Zhang et al., 2018b; Ma et al., 2018; Yang et al., 2018; Chen et al., 2019). Some studies have shown that the stagnation of meteorological conditions such as high relative humidity of the atmosphere, low mixed boundary layer height, low wind speed, and rapid chemical reactions leads to frequent pollution (Zhong et al., 2018a; Zhong et al., 2018b). On the other hand, some researchers proposed that the transformation of secondary aerosols promotes the explosive growth of $PM_{2.5}$ (Li et al., 2019; Wu et al., 2020; Dao et al., 2021; Rai et al., 2021; Wu et al., 2022). However, due to the diverse sources of air pollutants, complex chemical composition, and the coupling of various environmental factors, the polluted factors have not been fully quantified, and its chemical reaction mechanism is still controversial.

Water-soluble inorganic ions (WSIIs) are important chemical components in $PM_{2.5}$, accounting for up to 70% of the $PM_{2.5}$ mass concentration (Sun et al., 2019; Su et al., 2021). They exhibit strong hygroscopicity and can directly affect the acidity of atmospheric precipitation (Zhan et al., 2021). Among them, SO_4^{2-}, NO_3^-, and NH_4^+ (SNA) have a great influence on the atmospheric extinction coefficient and are important factors causing urban visibility degradation. Some studies showed that the high concentration of gaseous precursors tends to promote heterogeneous reactions on the $PM_{2.5}$ surface and forms secondary pollutants in haze days (Shao et al., 2019; Wang et al., 2020; Lei et al., 2021). Therefore, it is of great significance to study the concentration characteristics and sources of $PM_{2.5}$ and WSIIs for exploring the cause and control of $PM_{2.5}$.

In order to better understand the formation mechanism of $PM_{2.5}$ in Beijing, we conducted continuous observation of WSIIs in $PM_{2.5}$ during the heating season of 2021 in Beijing. $PM_{2.5}$ pollution is generally the worst during the heating season of a year (Pang et al., 2020; Dao et al., 2022). During this period, a high load of coal particles is generated and released into the atmosphere by the burning of coal for heating (Dao et al., 2022). In addition, low temperatures during the heating season slow down the dispersal of air pollutants, further exacerbating $PM_{2.5}$ pollution. The heating season of 2021 in Beijing lasted for about 5 months, from 28 October 2021 to 23 March 2022. During the heating season, Beijing hosted the XXIV Olympic Winter Games (from 4 February 2022 to 20 February 2022) and the XIII Paralympic Winter Games (from 4 March 2022 to 13 March 2022). Some studies evaluated the air pollution during the 2008 Olympic Games and proposed that atmospheric concentrations of PM_{10}, $PM_{2.5}$, NH_3, NO_2, SO_2, and the particulate ions NH_4^+, NO_3^-, SO_4^{2-}, Ca^{2+}, Mg^{2+}, and K^+ all decreased because of strict emission controls (Shen et al., 2011). While preparing and hosting the Winter Olympics, Beijing, Hebei, and other neighboring cities and provinces have been authorized to temporarily control enterprises and vehicles with heavy pollution, large emissions, and relatively little economic impact to create a favorable environment for hosting the games. Therefore, improved field observation on the Beijing's 2021 heating season can not only measure the impact of heating on $PM_{2.5}$ but also analyze the effects of emission reduction on $PM_{2.5}$. It would be beneficial to understanding the causes of pollution and helping the government to formulate effective measures to control air pollution.

2 Methods and data

2.1 Sampling site

Field measurements were performed on the roof of the building of the Chinese Academy of Meteorological Sciences (CAMS), approximately 53 m above the ground in the yard of the China Meteorological Administration (39°57′N, 116°19′E). The sampling site is located within the northwestern Third Ring Road of Beijing, around 200 m from the main road as shown in Figure 1. It is a typical urban observation station surrounded by traffic and residential emissions without an obvious industrial source nearby.

2.2 Instrument and measurements

From 25 October 2021 to 22 March 2022, major water-soluble inorganic ions (NO_3^-, SO_4^{2-}, Cl^-, NH_4^+, Na^+, K^+, Mg^{2+}, and Ca^{2+}) in $PM_{2.5}$ were continuously measured using an online Ambient Ion Monitor (AIM, model URG-9000D, United States) with 1-h time resolution. The ambient air was pumped through a $PM_{2.5}$ cyclone (at a flow rate of 3 l per minute), parallel plate denuder, steam-jet aerosol collector, aerosol sample collector, and then to two ion chromatographs (model ICS-1000, Dionex, United States) for chemical analysis (Hu et al., 2014). The interfering acidic and basic gases were removed in the parallel plate denuder by ultra-pure water with 0.018% vol H_2O_2. Aerosol particles were grown into liquid droplets inside the steam-jet aerosol collector due to supersaturated water vapor condensation on them. Also, these liquid droplets were collected by the aerosol sample collector until they were injected into ion chromatograph,

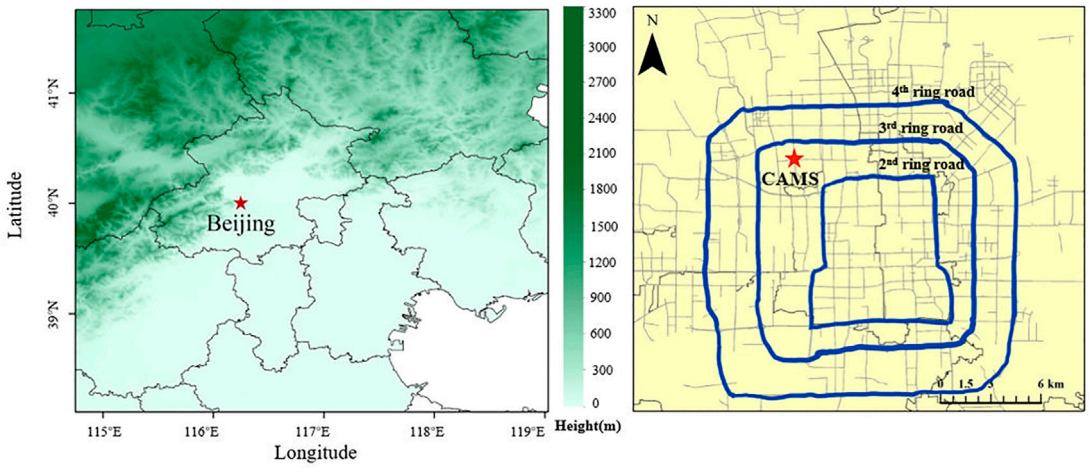

FIGURE 1
Geographical location of the observation site. The blue lines represent Beijing's main ring roads.

where the soluble species were analyzed. The chromatography conditions were as follows: CS12 analytical column, 22 mM MSA eluent, and cation self-regenerating suppressor for cations; AS22 analytical column, 4.5 mM Na_2CO_3/1.4 mM $NaHCO_3$ eluent, and anion self-regenerating suppressor for anions.

To ensure the accuracy of the measurements, the system was calibrated and maintained periodically. The temperature and pressure sensors were calibrated yearly to ensure the accuracy of sample volume. The ion chromatograph was calibrated monthly using standard anionic solutions (NO_3^-, SO_4^{2-}, and Cl^-) and cationic solutions (NH_4^+, Na^+, K^+, Mg^{2+}, and Ca^{2+}). Multi-point calibrations were considered qualified if the linear correlation of the standard curve of each ion was above 0.999. The minimum detection limit (MDL) was estimated by sampling zero air. The MDL for SO_4^{2-}, NO_3^-, and NH_4^+ was 0.0026, 0.047, and 0.013 μg/m^3, respectively. The MDL ranged from 0.002 to 0.307 μg/m^3 for other ions (Cl^-, Na^+, K^+, Mg^{2+}, and Ca^{2+}) (Hu et al., 2014). Membranes in the parallel plate denuder were changed once a month, and the in-line filters, which removed the insoluble particles in the samples, were replaced every 4–7 days.

The mass concentration of $PM_{2.5}$, PM_{10}, and trace gases (SO_2, O_3, and NO_2) used in this study was observed at the Guanyuan Monitoring Station by the China National Environmental Monitoring Center (CNEMC). The Guanyuan Monitoring Station is only 3 km away from our station. Both of them are Beijing urban stations with a similar surrounding environment.

The hourly meteorological data (air pressure, temperature, relative humidity, wind speed, and wind direction) in this study were obtained from the nearest meteorological data station, Haidian Meteorological Observation Station (No. 54399). It is about 5 km northwest to our sampling site, located inside Haidian Park, Beijing. To some extent, the data can represent meteorological conditions at our site.

All data in this study are reported in local time, 8 h ahead of UTC.

3 Results and discussion

3.1 Overview of the air quality during observation

In this study, the days with the daily average air quality index (AQI) greater than 100 were listed as the polluted days, while the days with the average daily AQI less than 50 were defined as the clean period. Time series of the daily mean AQI throughout the 2021 heating season is shown in Figure 2A. There were 17 polluted days (AQI >100) out of 147 days measured, according to the National Standard of the People's Republic of China "Ambient Air Quality Standard" (GB3095-2012). $PM_{2.5}$ was the major air pollutant in these 17 polluted days. Among them, three heavy polluted episodes were characterized by long duration and high daily mean value of AQI. The first heavy polluted episode occurred in the early heating season (from 15: 00 on 3 November 2021 to 03:00 on 6 November 2021) and lasted about 3 days with the hourly maximum AQI of 218. This polluted episode was preceded by a short period of a polluted process. The second polluted episode lasted more than 3 days from 23:00 on 21 January 2022 to 10:00 on 25 January 2022 with AQI rising from 112 to 215, which was about 2 weeks ahead of the start of the XXIV Olympic Winter Games. During the XXIV Olympic Winter Games, air quality was very good, with 10 days being excellent (0 < AQI <50) and 6 days being good (51 < AQI <100).

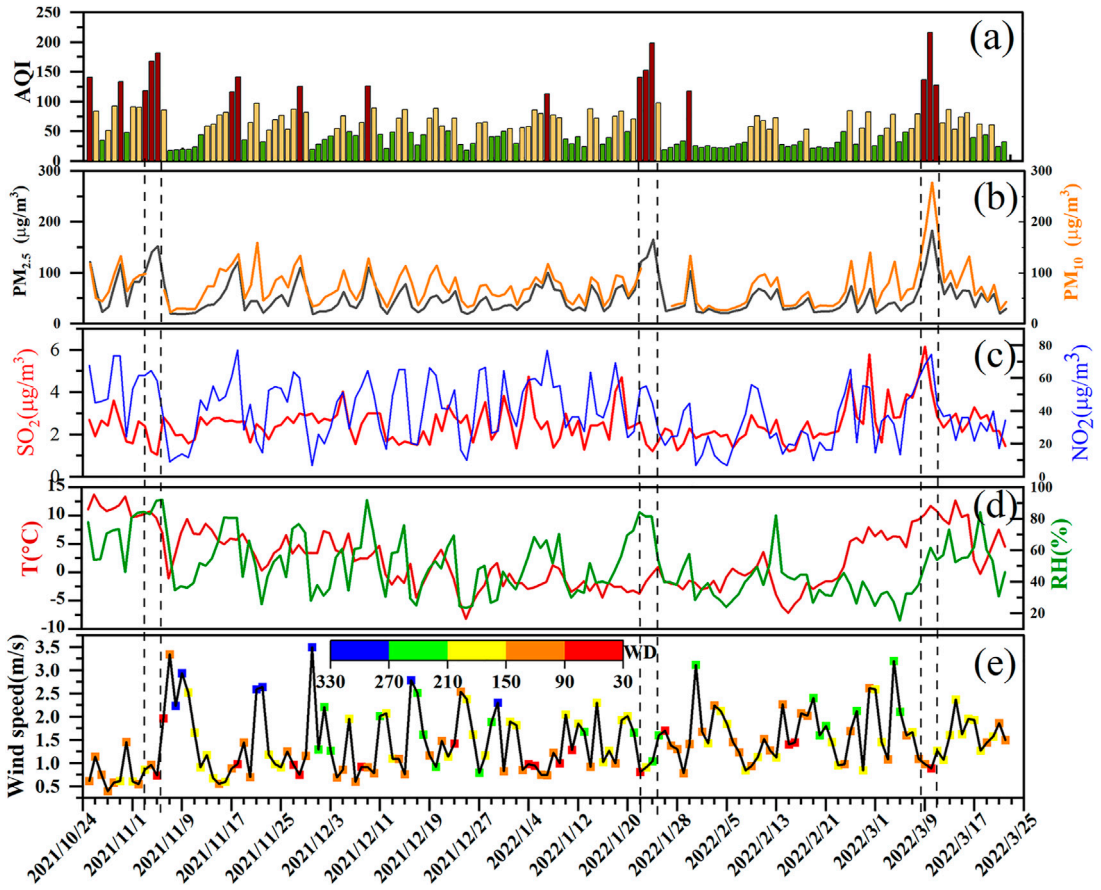

FIGURE 2
Time series of daily **(A)** mean air quality index (AQI); the green, yellow, and brown bars represent excellent day, good day, and polluted day, respectively; **(B)** time series of $PM_{2.5}$ and PM_{10} mass concentration; **(C)** SO_2 and NO_2 mass concentration; **(D)** ambient relative humidity (RH) and temperature (T); and **(E)** wind speed and wind direction (WD); three polluted episodes are highlighted by the black dashed lines.

The air quality during the XIII Paralympic Winter Games was not as good as that during XXIV Olympic Winter Games. There were only 2 days with excellent air quality. In addition, the third heavy polluted episode of the heating season occurred from 03:00 on 10 March 2022 to 03:00 on 11 March. This heavy polluted episode lasted for about 1 day, and the AQI reached its maximum for the entire heating season (hourly AQI reached 234). As shown in Figures 2B,C, the main pollutants in these three pollution episodes were $PM_{2.5}$ with high NO_2 concentrations.

3.2 Meteorological conditions

During the whole heating season of 2021 in Beijing, as shown in Figure 2D, the daily average temperature was low and the temperature span was large. This is shown in the summary of the hourly meteorological data in Table 1, and the mean temperature in the whole heating season was 2.4°C. The highest temperature reached 22.5°C, and the lowest temperature was as low as −10.9°C. The average temperature during the Olympic Winter Games was the lowest (−2.0°C), followed by the clean period (1.2°C) and polluted period (5.1°C). The average temperature during the Paralympic Winter Games was the highest, with a value of 8.5°C. In terms of wind speed, the whole heating season was dominated by light winds. Except for Paralympic Winter Games, the average wind speed was below 2.0 m/s during the clean period, polluted period, and Olympics Winter Games period. Particularly in the polluted period, the wind speed was much lower, and the average wind speed was only 1.0 m/s. As shown in Figure 2E, the polluted period was dominated by south and southwest winds, while the clean period was characterized by north winds, often fluctuating between 0.6 and 4.0 m/s. Winds from the southwest or southeast often bring high concentrations of $PM_{2.5}$, while clean air comes mostly from the northwest, effectively removing air pollution in Beijing (Li et al., 2021; Su et al., 2021).

TABLE 1 Hourly meteorological factors, hourly mass concentration of $PM_{2.5}$ and its water-soluble inorganic ions during the clean period, polluted period, Olympics Winter Games period, and Paralympics Winter Games period.

	Heating season			Clean period			Polluted period			Olympics Winter Games period			Paralympics Winter Games period		
	Min	Max	Mean	Min	Max	Mean	Min	Max	Mean	Min	Max	Mean	Min	Max	Mean
T (°C)	-10.9	22.5	2.4	-10.9	22.5	1.2	-8.5	21.1	5.1	-10.9	10.4	-2.0	-2.9	19.8	8.5
RH (%)	8.0	99.0	50.1	8.0	97.0	36.4	13.0	99.0	74.9	14.0	93.0	41.2	8.0	94.0	42.5
WS (m/s)	0.0	7.7	1.5	0.1	7.7	1.8	0.0	6.5	1.0	0.0	5.9	1.6	0.0	6.5	1.5
$PM_{2.5}$	2.0	201.0	36.9	2.0	48.0	10.8	36.0	201.0	109.8	4.0	97.0	23.3	4.0	195	61.4
NO_3^-	0.01	52.8	6.1	0.01	15.5	1.2	0.3	52.8	22.9	0.1	16.4	3.5	0.01	48.6	13.4
SO_4^{2-}	0.01	17.8	1.7	0.2	4.9	0.8	0.7	17.8	5.2	0.5	7.9	1.8	0.2	7.2	2.0
Cl^-	0.1	3.0	0.7	0.03	2.7	0.5	0.1	3.0	1.3	0.2	2.4	0.7	0.4	2.5	1.0
NH_4^+	0.1	19.2	1.9	0.01	5.5	0.3	0.1	19.2	8.0	0.1	4.3	1.1	0.1	13.0	3.7
Na^+	0.3	4.4	1.5	0.5	4.4	1.6	0.3	3.0	1.3	0.7	1.6	0.9	0.7	1.6	1.0
K^+	0.004	3.0	0.2	0.005	3.0	0.1	0.04	1.1	0.3	0.01	0.2	0.1	0.01	0.3	0.1
Mg^{2+}	0.008	2.4	0.2	0.006	2.4	0.2	0.02	1.0	0.3	0.1	0.6	0.1	0.1	0.6	0.3
Ca^{2+}	0.1	6.4	2.2	0.1	5.6	1.9	0.4	5.3	2.5	1.0	2.0	1.2	1.2	6.4	1.8

The mass concentration unit of $PM_{2.5}$ and water-soluble inorganic ions is $\mu g/m^3$.

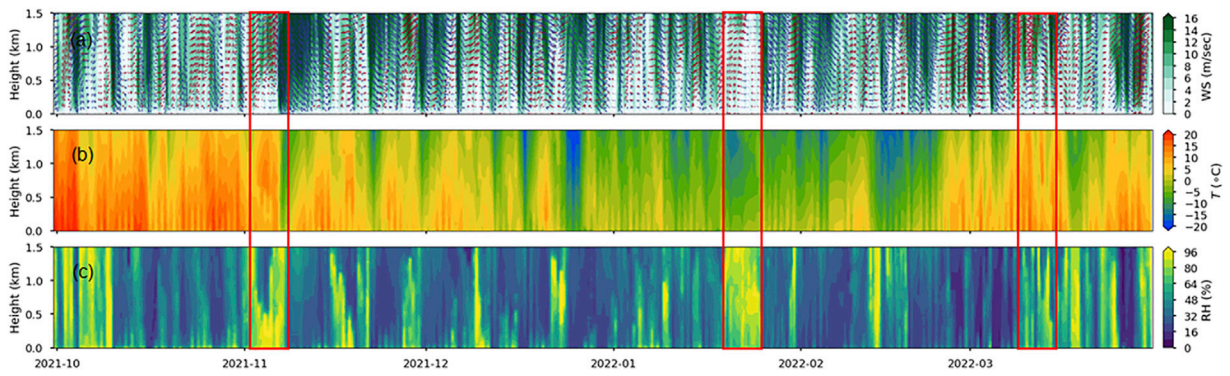

FIGURE 3
Time series of vertical distribution of meteorological factors including **(A)** wind speed; **(B)** temperature (T); and **(C)** relative humidity (RH) from 25 October 2021 to 22 March 2022; the solid red line represents the three polluted episodes.

It can be seen from Figure 2D that heavy pollution usually occurred with relatively high temperature or high humidity in winter. In the early heating season in Beijing (2 November 2021–6 November 2021), the first polluted episode occurred, during which the southwest wind was dominated, the hourly average temperature was 10.4°C, and the average RH was 87%. By the end of this polluted episode (23:00 on 6 November 2021), the wind turned to northwest, with the hourly maximum wind speed of 4.7 m/s, and then the air quality ameliorated. This is due to the fact that strong winds blow away pollutants quickly (Zhao et al., 2019; Han et al., 2020). The second polluted episode occurred after a snowfall on 20 January 2022. This episode lasted for more than 3 days (23:00 on 21 January 2022–10:00 on 25 January 2022), with the hourly average temperature which reached 11.1°C, RH which reached 81.8%, and the wind speed was only 1.1 m/s. Low wind speed was not conducive to the

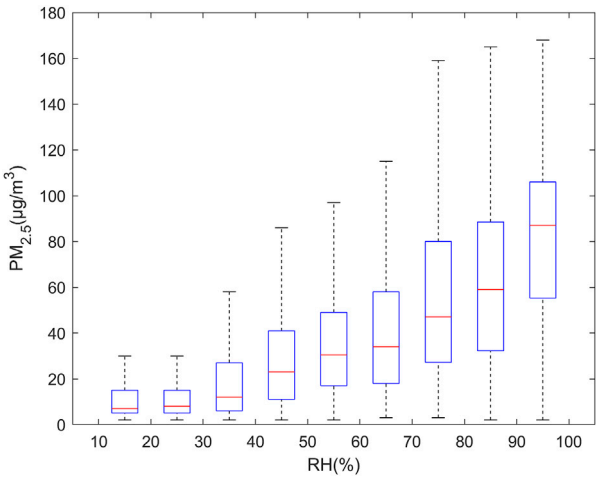

FIGURE 4
Relationship between $PM_{2.5}$ mass concentration and RH in the heating season.

diffusion of pollutants (Wu et al., 2020). The RH in the first and second polluted episodes was high (>80%). In the third polluted episode, the RH was around 60%. It can also be seen from Table 1 that the average RH in the polluted period was 1.5 times larger than the average RH of the whole heating season and 2.1 times larger than that in the clean period.

The vertical distribution of meteorological factors (wind speed, temperature, and relative humidity) from surface up to 1.5 km is shown in Figure 3. As shown in Figure 3A, the wind speed near the ground was low, indicating that it is not conducive to the diffusion of pollutants throughout the whole heating season. It is also worth noting that the air quality would deteriorate once the humidity increased. In Figure 3B, there was a significant temperature inversion in the first and third polluted episodes. As can be seen from Figure 3C, the RH near the ground was above 60% in the three polluted episodes and the early heating season when the pollution occurred frequently. In contrast, the RH in the clean periods was low, which further confirmed that the RH was higher in the polluted periods not only at the surface but also in the upper air.

3.3 $PM_{2.5}$ mass concentration

In this study, the characteristics of $PM_{2.5}$ mass concentration in the 2021 heating season in Beijing were explored. Table 1 shows the statistical results of hourly $PM_{2.5}$ mass concentration during the heating period including the polluted period, the clean period, the XXIV Olympic Winter Games period, and the XIII Paralympic Winter Games period. The hourly mean $PM_{2.5}$ mass concentration during the heating season was 36.9 μg/m^3, which was close to the excellent standard for $PM_{2.5}$ mass concentration (35.0 μg/m^3) in accordance with the Chinese National Ambient Air Quality Standard (GB 3095–2012). During the clean period, the hourly average mass concentration of $PM_{2.5}$ was 10.8 μg/m^3. During the heating period, the highest hourly mass concentration of $PM_{2.5}$ reached 201.0 μg/m^3, which was 5.7 times the national standard (GB3095-2012, 35.0 μg/m^3). While during the Olympic Winter Games, the hourly concentration of $PM_{2.5}$ ranged from 4.0 to 97.0 μg/m^3, with no obvious pollution, and the overall air quality was good, with an average mass concentration of 23.3 μg/m^3. The mass concentration of $PM_{2.5}$ was in the range of 4.0–195.0 μg/m^3 during the Paralympic Winter Games, and the average mass concentration was 61.4 μg/m^3, which was 2.6 times that of the Olympic Winter Games.

RH had a great influence on the formation of pollution; higher RH promoted the growth of the mass concentration of $PM_{2.5}$ (Wu et al., 2022). As displayed in Figure 4, $PM_{2.5}$ mass concentration increased with the increase in RH. When RH was below 40%, $PM_{2.5}$ mass concentration changed slowly with RH. However, when RH was greater than 40%, especially above 60%, $PM_{2.5}$ increased sharply with the increase in RH. Higher relative humidity was believed to increase the content of liquid water on the surface of particles and even cause deliquescence, thus promoting some aqueous-phase reactions on the aerosol surface (Herrmann et al., 2015; Wu et al., 2019). In this case, trace gases such as SO_2 and NO_2 in the atmosphere may be converted into secondary aerosols through aqueous-phase reactions, thus aggravating $PM_{2.5}$ pollution (Sun et al., 2013; Zhong et al., 2017).

3.4 Water-soluble inorganic ions (WSIIs)

$PM_{2.5}$ contains a large number of WSIIs including SO_4^{2-}, NO_3^-, Cl^-, NH_4^+, Na^+, K^+, Mg^{2+}, and Ca^{2+}. The proportions of each ionic component in the clean period and the polluted period are shown in Figure 5. The concentration of WSIIs accounted for 38.2% of $PM_{2.5}$ in the polluted period, while it can be as high as 61.4% during the clean period. The proportion of SNA in $PM_{2.5}$ increased with the increase in pollution (Zhan et al., 2021). SNA accounted for 20%–83% of the total mass WSIIs during the clean period and 22%–96% during the polluted period with the average of 83.1%. Over the whole heating season, the hourly mean mass concentration of sulfate, nitrate, and ammonium was 1.7 μg/m^3, 6.1 μg/m^3, and 1.9 μg/m^3, respectively. Compared with the winter SNA mass concentration of 2013–2017, the SNA concentration of 2021 was reduced (Wang et al., 2019a). The proportions of sulfate, nitrate, and ammonium in $PM_{2.5}$ in the clean period were 7.4%, 11.1%, and 2.5% and in the polluted period were 4.8%, 21%, and 7.3%, respectively. During the XXIV Olympic Winter Games period, the WSII mass concentration accounted for 40.3% of $PM_{2.5}$. SNA contributed to 7.7%, 15%, and 4.7% of the total mass WSIIs, respectively. The WSII mass concentration contributed to 38.0% of $PM_{2.5}$ mass concentration in the Paralympics Winter

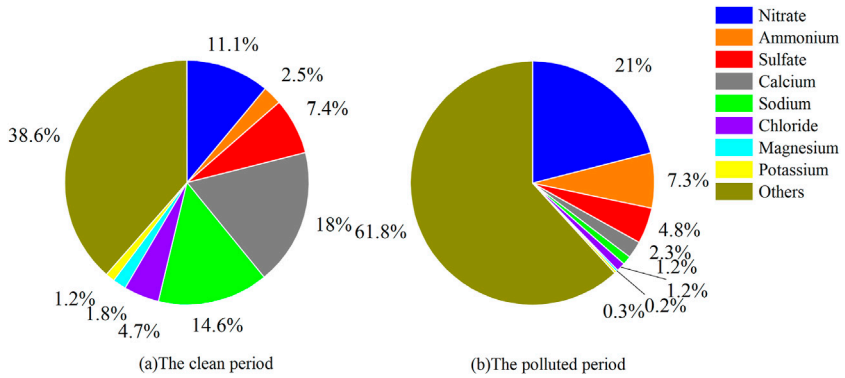

FIGURE 5
Percentage of water-soluble inorganic ions (WSIIs) in $PM_{2.5}$ mass concentration. **(A)** clean period and **(B)** polluted period.

Games period, while SNA accounted for 6.0%, 21.8%, and 3.3%, respectively.

Although the proportion of WSIIs was low in $PM_{2.5}$ during the polluted period compared to the clean period, the overall concentration of WSIIs was higher than that in the clean period. In the clean period, the hourly mean mass concentration of WSIIs was 6.6 μg/m^3, while it was 41.8 μg/m^3 in the polluted period. As shown in Table 1, the hourly average mass concentration of WSIIs in the polluted period was in the following order: NO_3^- > NH_4^+> SO_4^{2-} > Ca^{2+}> Na^+> Cl^- > Mg^{2+}> K^+. During both the clean and polluted periods, the concentration of NO_3^- was the highest among all WSIIs. The hourly average mass concentration of NO_3^- during the polluted period was 22.9 μg/m^3, which was 19.1 times of that in the clean period (1.2 μg/m^3). As for SO_4^{2-}, the mean mass concentration in the polluted period (5.2 μg/m^3) was 6.5 times of that in the clean period (0.8 μg/m^3). NH_4^+ mean mass concentration was 8.0 μg/m^3 and 0.3 μg/m^3 in the polluted and clean periods, respectively. In contrast, the concentrations of Na^+, K^+, Mg^{2+}, Ca^{2+}, and Cl^- in $PM_{2.5}$ were lower. Throughout the heating season, the hourly maximum concentrations of Ca^{2+} and Mg^{2+}, which were mainly from dust, were 6.4 μg/m^3 and 2.4 μg/m^3, respectively. Cl^- mass concentrations fluctuated between 0.1 and 3.0 μg/m^3, while K^+ was usually used as a tracer for biomass burning (Wu et al., 2019), with an hourly average concentration of 0.2 μg/m^3, which was the lowest concentration among WSIIs.

During the Olympics Winter Games period, no polluted episode occurred, and the hourly mean mass concentrations of sulfate, nitrate, and ammonium were 1.8 μg/m^3, 3.5 μg/m^3, and 1.1 μg/m^3, respectively. While the third polluted episode occurred during the Paralympic Winter Games period, a dusty event (9 March 2022–10 March 2022) occurred, and the hourly maximum concentration of Ca^{2+} reached 6.4 μg/m^3. Also, during this episode, the hourly maximum concentration of NO_3^-, SO_4^{2-}, and NH_4^+ reached 48.6 μg/m^3, 7.2 μg/m^3, and 13.0 μg/m^3, respectively. The concentration of sulfate, nitrate, and ammonium during the Paralympic Winter Games period was 1.1, 3.8, and 3.4 times that of the Olympics Winter Games period.

Figure 6 displays time series of major WSII mass concentrations during the filed observation. The variation trend of SNA and $PM_{2.5}$ mass concentration was similar. The peaks and valleys of most SNA and $PM_{2.5}$ basically appeared at the same time. SNA occupied the largest fraction in WSIIs; SNA accounted for 68.1% of the WSIIs during the Olympics Winter Games and 82.0% during the Paralympics Winter Games. This indicates that with the increase in pollution, SNA contributed more, which was roughly similar to the observation of Xu et al. (2019a) during the Asia Pacific Economic Cooperation Summit (APEC). The concentration of WSIIs in the clean period was lower than that in the polluted period. The concentrations of Mg^{2+} and Na^+ in the polluted period were lower and the fluctuation was smaller than those in the clean period. The mass concentrations of Ca^{2+} and Cl^- increased with the increase in pollution.

3.5 Secondary aerosol processes

The secondary transformation process plays an important role in the formation of SNA in $PM_{2.5}$ (Wang et al., 2021). The mass ratio of $PM_{2.5}$/CO is often used to qualitatively evaluate the intensity of secondary transformation of $PM_{2.5}$ to exclude the impact of primary combustion emissions and meteorological conditions (He et al., 2017; Wu et al., 2020). In this study, the hourly ratio of $PM_{2.5}$/CO in Beijing was 0.03 ± 0.01 during the clean period and 0.10 ± 0.03 in the polluted period, which was 3.3 times that of the clean period, indicating that the secondary pollution in the polluted period was aggravated. Figure 7 shows that $PM_{2.5}$/CO increased significantly during the polluted period, especially during the three polluted episodes.

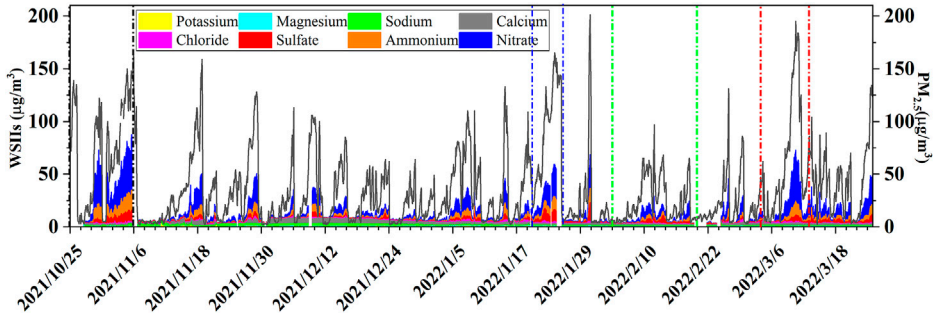

FIGURE 6
Time series of $PM_{2.5}$ and WSIIs mass concentration; the black dotted lines are the test heating time; the blue dotted lines represent snowfall; the green dotted lines represent the Olympic Winter Games period, and the red lines represent the Paralympic Winter Games period.

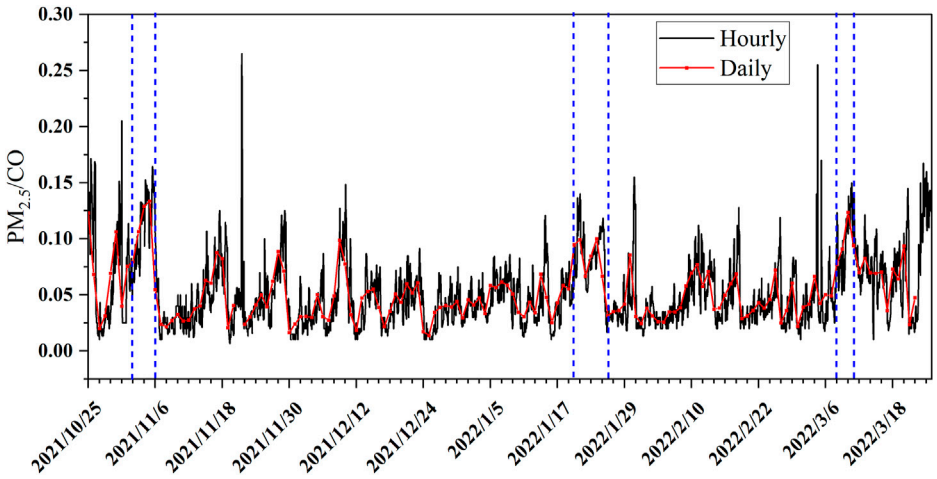

FIGURE 7
Time series of hourly and daily $PM_{2.5}$/CO mass ratios; the three polluted episodes are marked by blue dashed lines.

To further explore the secondary transformation process, the sulfur oxidation ratio (SOR) and nitrogen oxidation ratio (NOR) are usually used to quantitatively study the secondary conversion reactions of SO_2 and NO_2 to form sulfate and nitrate, respectively (Li et al., 2018; Li et al., 2019; Zhao et al., 2019; Yang et al., 2022). They were calculated as follows:

$$\mathrm{SOR} = \frac{\mathrm{n}[\mathrm{SO_4^{2-}}]}{\mathrm{n}[\mathrm{SO_4^{2-}}] + \mathrm{n}[\mathrm{SO_2}]},$$
$$\mathrm{NOR} = \frac{\mathrm{n}[\mathrm{NO_3^{-}}]}{\mathrm{n}[\mathrm{NO_3^{-}}] + \mathrm{n}[\mathrm{NO_2}]}, \quad (1)$$

where n refers to the molar concentration.

The higher SOR and NOR suggested that greater oxidation of gaseous species would occur and secondary aerosols would be formed in the atmosphere (Fu et al., 2008). Generally, when their values were >0.10, secondary transformation processes such as photochemical oxidation and heterogeneous reactions would play an important role in the formation of sulfate and nitrate from gas-phase SO_2 and NOx. Nitrate and sulfate are suggested to be mainly generated from the primary emission sources if NOR and SOR values are less than 0.1 (Xu et al., 2019a).

The SOR in the clean period was 0.22, while the SOR in the polluted period was 0.55. The mean SOR for both clean and polluted periods was greater than 0.1, indicating that the secondary transformation was the primary source of SO_4^{2-} formation. The formation of SO_4^{2-} in the atmosphere proposed by previous studies mainly includes the gas-phase oxidation of SO_2 by OH radicals and the aqueous oxidation of H_2O_2, O_3, and NO_2 to S (VI) and the catalytic oxidation by

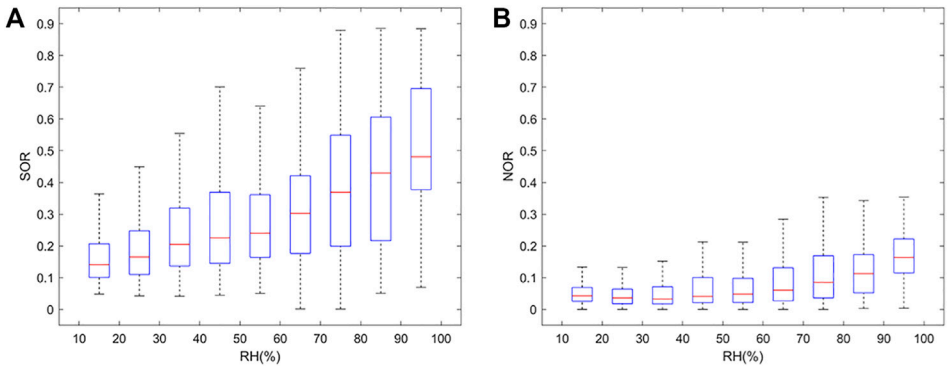

FIGURE 8
Relationship between **(A)** SOR and relative humidity; **(B)**NOR and relative humidity.

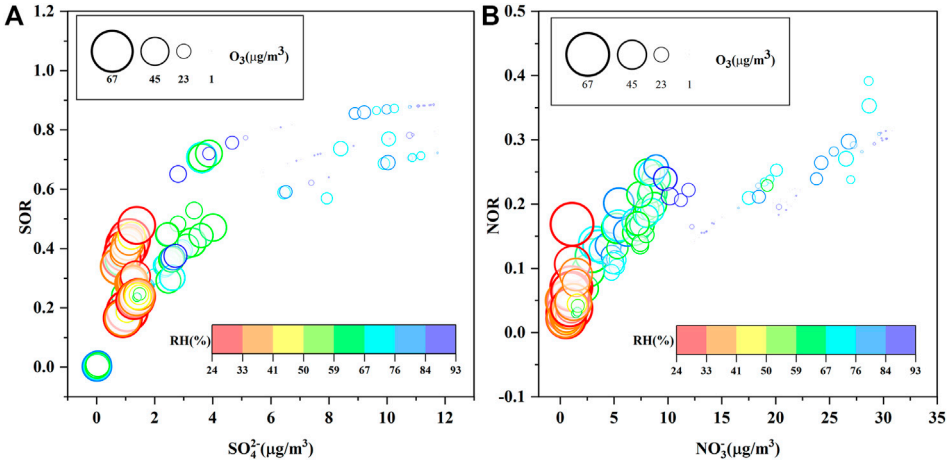

FIGURE 9
(A) Relationship between SOR and SO_4^{2-} colored by RH and **(B)** relationship between NOR and NO_3^- colored by RH; the circle size represents the O_3 mass concentration. The data used in this figure were from January 20 to January 26, 2022 (there were snowfalls during January 20–23).

transition metals such as Fe^{3+} and Mn^{2+} in cloud droplets and aerosols (Dong et al., 2020; Cao et al., 2021). The SOR in this study showed a clearly increasing trend with RH (shown in Figure 8A). When RH > 60%, the SOR increased faster. This possibly suggested that the aqueous oxidation of SO_2 to produce SO_4^{2-} is enhanced under high RH conditions due to high liquid water content in the aerosol (Zhang et al., 2018a; Wu et al., 2022).

In order to further explore the mechanism of sulfate and nitrate formation under high RH, we selected the second polluted episode with a snowfall event (from January 20 to January 26, 2022) as a case for detailed analysis. There were intermittent snowfalls in Beijing from January 20 to 23. After the snowfall stopped, the RH was high and the pollution continued to aggravate. As shown in Figure 6, the $PM_{2.5}$ hourly mass concentration climbed from 73.0 to 165.0 μg/m^3 during the second episode. The NO_3^- hourly mass concentration increased rapidly from 12.5 to 30.8 μg/m^3, while the sulfate hourly mass concentration rose from 4.6 to 11.9 μg/m^3. It was interesting to observe from Figure 9A that the SOR increased with the increase in sulfate mass. When SO_4^{2-} < 2 μg/m^3, O_3 promoted the formation of sulfate to some extent, and the SOR increased with O_3 concentration. However, O_3 had little influence on sulfate formation when the sulfate concentration increased. The concentration of O_3 decreased, but the SOR value still grew up. At the same time, it was found that high SOR and sulfate values both appeared at high relative humidity, especially above 60%. O_3 and RH were believed to be two factors in the formation of sulfate (Fang et al., 2019). Previous studies proposed that sulfate formation mechanisms in the atmosphere primarily include gas-phase oxidation of SO_2 by OH radicals and the

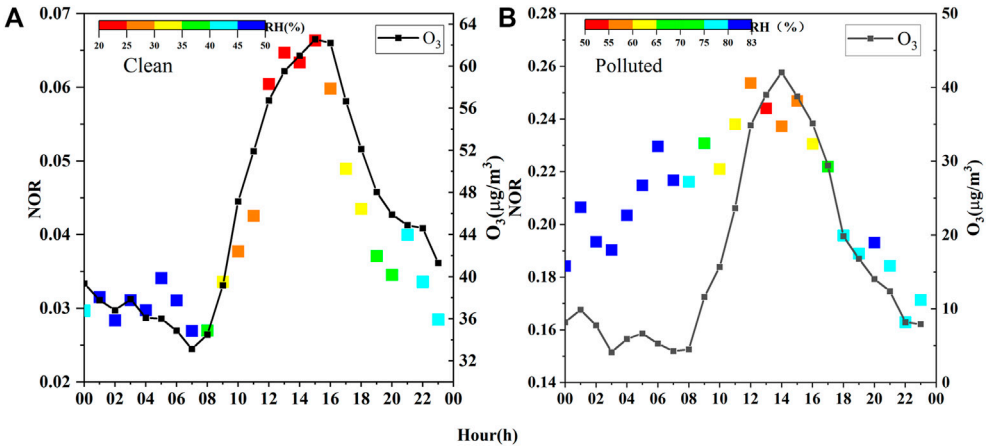

FIGURE 10
Diurnal variation of O_3 and NOR colored by RH **(A)** during the clean period and **(B)** during the polluted period.

aqueous oxidation of S(IV) by H_2O_2, O_3, organic peroxides, and NO_2 and catalytic oxidation by transition metal ions (TMIs), for example, Fe(III) and Mn(II), in cloud/fog water droplets (Li et al., 2020; Wang et al., 2021; Wang et al., 2022b; Wang et al., 2022c; Wang et al., 2022d; Gao et al., 2022; Ye et al., 2022). As sulfate itself exhibit strong hygroscopicity (Kong et al., 2020), with the increase in sulfate and RH, the $PM_{2.5}$ surface water content would increase, which would be more conducive to potential aqueous oxidation of S(IV), resulting in the increase in SOR. This can partly explain the aforementioned fact that RH and O_3 affect the secondary transformation process.

Fu et al. proposed that the NOR was less than 0.1 in the case when nitrate was mainly generated from primary emissions and greater than 0.1 when nitrate was mainly generated through the secondary transformation of NOx oxidation (Fu et al., 2008). The mean NOR value in the clean period was 0.04 and in the polluted period was 0.21, suggesting that nitrate was mainly formed by secondary transformation processes in the polluted period and by primary emission sources in the clean period. RH and O_3 can affect these secondary transformation processes in the polluted period. As shown in Figure 8B, NOR rose with the increase in RH although the effect of RH was less than that of SOR. When the RH was less than 60%, most values of the NOR were less than 0.1. When the RH was more than 60%, the NOR began to rise, and the average values were above 0.1. It indicated that higher RH may promote nitrate formation. The relationship between NOR and NO_3^- with O_3 and RH is shown in Figure 9B. NOR presented an upward trend with the increase in NO_3^-. At high relative humidity, the NOR increased with nitrate concentration and was greater than 0.1 even at low O_3 concentrations. Heterogeneous hydrolysis of N_2O_5 under high humidity conditions may contribute to the formation of HNO_3 at night (Yun et al., 2018; Chen et al., 2020; Yang et al., 2022).

The diurnal variation of O_3 concentration and NOR in the clean and polluted periods is shown in Figures 10A, B, respectively, as well as their relationship with RH. It can be seen from Figure 10A that the diurnal variation of O_3 mass concentration and NOR showed a similar trend during the clean period. They presented an obvious single peak and reached the maximum around 15:00. However, in the polluted period, NOR only maintained a good consistency with O_3 concentration in the afternoon, as shown in Figure 10B. Due to the weakening of the titration effect of NOx, the increase in O_3 concentration leads to the enhancement of atmospheric oxidation capacity, promoting the formation of NOx to HNO_3, and then reacted with NH_3 in the atmosphere to form nitrate (Ren et al., 2021). However, at night, the NOR still rose when O_3 concentration decreased. In addition, it was found that the NOR increased with the increase in RH. According to the studies in previous literatures, heterogeneous hydrolysis of N_2O_5 may contribute to the formation of HNO_3 at night under high humidity conditions (Zhang et al., 2018a; Wang et al., 2022a).

4 Conclusion

Hourly mass concentrations of water-soluble inorganic ions in $PM_{2.5}$ were continuously measured in Beijing during the entire 2021 heating season, which covered not only the 2021 winter but also the periods of XXIV Olympic Winter Games and XIII Paralympic Winter Games. The filed observation lasted for about 5 months from 25 October 2021 to 22 March 2022. This study analyzed the characteristics of $PM_{2.5}$ and WSII mass concentrations during this period and investigated the influence of meteorological conditions on their formation. It was found that meteorological factors played an important role in the $PM_{2.5}$ pollution. Most of the polluted processes occurred

under conditions of low wind speed, temperature inversion, and high RH, which were in favor of local accumulation of pollutants and secondary transformation. The $PM_{2.5}$/CO ratio, an indicator of the contribution of secondary aerosols to $PM_{2.5}$, suggested that the secondary conversion was enhanced in the polluted period.

Total mass concentration of WSIIs accounted for 38.2% and 61.4% in the polluted and clean periods, respectively. Among them, during the polluted period, the average contribution of SNA to WSIIs was 83.1%. The concentration of nitrate was the highest in WSIIs. The SOR and NOR in the polluted period were much higher than those in the clean period, which further confirmed that the secondary transformation process had an important impact on the occurrence of $PM_{2.5}$ pollution. In addition, high RH was conducive to the formation of secondary aerosols such as sulfate, which further aggravated pollution. For secondary aerosols such as nitrate, heterogeneous hydrolysis of N_2O_5 under high humidity conditions may contribute to the formation of nitrate at night in the polluted period, while photochemical reactions were another pathway of nitrate formation during the day.

Data availability statement

All data given in figures are displayed in tables or in digital form. Readers who are interested in the data should contact the corresponding authors.

Author contributions

JW: field investigation, analyzed the observational data and prepared the figures of the manuscript, draft the manuscript. LW: conceptualization, methodology, data analysis, revising—original draft, funding acquisition, and guiding the field investigation. JS: conceptualization, writing—review and editing, supervision, funding acquisition. JW, SZ and LW performed the instrument deployment and operation. SZ: field investigation. JZ: plotting some figures. All co-authors discussed the results and commented on the manuscript.

Funding

This work was supported by the Beijing Natural Science Foundation (No. 8202052), the National Natural Science Foundation of China (Nos. 21777191, 42075082, and 41875147), and the Chinese Academy of Meteorological Sciences (2020KJ001, 2020Z002, and 2022KJ002). It was also supported by the Innovation Team for Haze-fog Observation and Forecasts of the Ministry of Science and Technology of the People's Republic of China and China Meteorological Administration.

Conflict of interest

The authors declare that the research was conducted in the absence of any commercial or financial relationships that could be construed as a potential conflict of interest.

Publisher's note

References

Cao, J., Qiu, X., Gao, J., Wang, F., Wang, J., Wu, J., et al. (2021). Significant decrease in SO_2 emission and enhanced atmospheric oxidation trigger changes in sulfate formation pathways in China during 2008–2016. *J. Clean. Prod.* 326, 129396. doi:10.1016/j.jclepro.2021.129396

Chen, X., Wang, H., Lu, K., Li, C., Zhai, T., Tan, Z., et al. (2020). Field determination of nitrate formation pathway in winter beijing. *Environ. Sci. Technol.* 54 (15), 9243–9253. doi:10.1021/acs.est.0c00972

Chen, Z., Chen, D., Wen, W., Zhuang, Y., Kwan, M.-P., Chen, B., et al. (2019). Evaluating the "2+26" regional strategy for air quality improvement during two air pollution alerts in beijing: Variations in $PM_{2.5}$ concentrations, source apportionment, and the relative contribution of local emission and regional transport. *Atmos. Chem. Phys.* 19 (10), 6879–6891. doi:10.5194/acp-19-6879-2019

Dao, X., Di, S. Y., Zhang, X., Gao, P. J., Wang, L., Yan, L. Y., et al. (2022). Composition and sources of particulate matter in the Beijing-Tianjin-Hebei region and its surrounding areas during the heating season. *Chemosphere* 291, 132779. doi:10.1016/j.chemosphere.2021.132779

Dao, X., Di, S., Zhang, X., Gao, P., Wang, L., Yan, L., et al. (2021). Composition and sources of particulate matter in the Beijing-Tianjin-Hebei region and its surrounding areas during the heating season. *Chemosphere* 291, 132779. doi:10.1016/j.chemosphere.2021.132779

Dong, C., Li, J., and Qi, Y. (2022). Decomposing $PM_{2.5}$ air pollution rebounds in Northern China before COVID-19. *Environ. Sci. Pollut. Res.* 29 (19), 28688–28699. doi:10.1007/s11356-021-17889-2

Dong, Z., Su, F., Zhang, Z., and Wang, S. (2020). Observation of chemical components of PM2.5 and secondary inorganic aerosol formation during haze and sandy haze days in Zhengzhou, China. *J. Environ. Sci.* 88, 316–325. doi:10.1016/j.jes.2019.09.016

Elser, M., Huang, R.-J., Wolf, R., Slowik, J. G., Wang, Q., Canonaco, F., et al. (2016). New insights into $PM_{2.5}$ chemical composition and sources in two major cities in China during extreme haze events using aerosol mass spectrometry. *Atmos. Chem. Phys.* 16 (5), 3207–3225. doi:10.5194/acp-16-3207-2016

Fang, Y., Ye, C., Wang, J., Wu, Y., Hu, M., Lin, W., et al. (2019). RH and O_3 concentration as two prerequisites for sulfate formation. *Atmos. Chem. Phys.* 19 (19), 12295–12307. doi:10.5194/acp-19-12295-2019

Fu, Q., Zhuang, G., Wang, J., Xu, C., Huang, K., Li, J., et al. (2008). Mechanism of formation of the heaviest pollution episode ever recorded in the Yangtze River

Delta, China. *Atmos. Environ. X.* 42 (9), 2023–2036. doi:10.1016/j.atmosenv.2007.12.002

Gao, J., Shi, G. L., Zhang, Z. C., Wei, Y. T., Tian, X., Feng, Y. C., et al. (2022). Targeting atmospheric oxidants can better reduce sulfate aerosol in China: H_2O_2 aqueous oxidation pathway dominates sulfate formation in haze. *Environ. Sci. Technol.* 56 (15), 10608–10618. doi:10.1021/acs.est.2c01739

Geng, G., Zheng, Y., Zhang, Q., Xue, T., Zhao, H., Tong, D., et al. (2021). Drivers of PM2.5 air pollution deaths in China 2002–2017. *Nat. Geosci.* 14 (9), 645–650. doi:10.1038/s41561-021-00792-3

Han, X., Guo, Q., Lang, Y., Li, S., Li, Y., Guo, Z., et al. (2020). Seasonal and long-term trends of sulfate, nitrate, and ammonium in $PM_{2.5}$ in beijing: Implication for air pollution control. *Environ. Sci. Pollut. Res.* 27 (19), 23730–23741. doi:10.1007/s11356-020-08697-1

He, J., Gong, S., Yu, Y., Yu, L., Wu, L., Mao, H., et al. (2017). Air pollution characteristics and their relation to meteorological conditions during 2014-2015 in major Chinese cities. *Environ. Pollut.* 223, 484–496. doi:10.1016/j.envpol.2017.01.050

Herrmann, H., Schaefer, T., Tilgner, A., Styler, S. A., Weller, C., Teich, M., et al. (2015). Tropospheric aqueous-phase chemistry: Kinetics, mechanisms, and its coupling to a changing gas phase. *Chem. Rev.* 115 (10), 4259–4334. doi:10.1021/cr500447k

Hu, G., Zhang, Y., Sun, J., Zhang, L., Shen, X., Lin, W., et al. (2014). Variability, formation and acidity of water-soluble ions in $PM_{2.5}$ in Beijing based on the semi-continuous observations. *Atmos. Res.* 145, 1–11. doi:10.1016/j.atmosres.2014.03.014

Hu, S., Zhao, G., Tan, T., Li, C., Zong, T., Xu, N., et al. (2021). Current challenges of improving visibility due to increasing nitrate fraction in $PM_{2.5}$ during the haze days in Beijing, China. *Environ. Pollut.* 290, 118032. doi:10.1016/j.envpol.2021.118032

Huang, X., Liu, Z., Zhang, J., Wen, T., Ji, D., and Wang, Y. (2016). Seasonal variation and secondary formation of size-segregated aerosol water-soluble inorganic ions during pollution episodes in Beijing. *Atmos. Res.* 168, 70–79. doi:10.1016/j.atmosres.2015.08.021

Huang, X., Tang, G., Zhang, J., Liu, B., Liu, C., Zhang, J., et al. (2021). Characteristics of $PM_{2.5}$ pollution in Beijing after the improvement of air quality. *J. Environ. Sci.* 100, 1–10. doi:10.1016/j.jes.2020.06.004

Kong, L., Feng, M., Liu, Y., Zhang, Y., Zhang, C., Li, C., et al. (2020). Elucidating the pollution characteristics of nitrate, sulfate and ammonium in $PM_{2.5}$ in Chengdu, southwest China, based on 3-year measurements. *Atmos. Chem. Phys.* 20 (19), 11181–11199. doi:10.5194/acp-20-11181-2020

Lachatre, M., Fortems-Cheiney, A., Foret, G., Siour, G., Dufour, G., Clarisse, L., et al. (2019). The unintended consequence of SO_2 and NO_2 regulations over China: Increase of ammonia levels and impact on $PM_{2.5}$ concentrations. *Atmos. Chem. Phys.* 19 (10), 6701–6716. doi:10.5194/acp-19-6701-2019

Lei, L., Zhou, W., Chen, C., He, Y., Li, Z., Sun, J., et al. (2021). Long-term characterization of aerosol chemistry in cold season from 2013 to 2020 in Beijing, China. *Environ. Pollut.* 268, 115952. doi:10.1016/j.envpol.2020.115952

Li, J., Gao, W., Cao, L., Xiao, Y., Zhang, Y., Zhao, S., et al. (2021). Significant changes in autumn and winter aerosol composition and sources in Beijing from 2012 to 2018: Effects of clean air actions. *Environ. Pollut.* 268, 115855. doi:10.1016/j.envpol.2020.115855

Li, J., Zhang, Y. L., Cao, F., Zhang, W., Fan, M., Lee, X., et al. (2020). Stable sulfur isotopes revealed a major role of transition-metal ion-catalyzed SO_2 oxidation in haze episodes. *Environ. Sci. Technol.* 54 (5), 2626–2634. doi:10.1021/acs.est.9b07150

Li, W., Liu, X., Zhang, Y., Tan, Q., Feng, M., Song, M., et al. (2019). Insights into the phenomenon of an explosive growth and sharp decline in haze: A case study in beijing. *J. Environ. Sci.* 84, 122–132. doi:10.1016/j.jes.2019.04.015

Li, X., Li, S., Xiong, Q., Yang, X., Qi, M., Zhao, W., et al. (2018). Characteristics of $PM_{2.5}$ chemical compositions and their effect on atmospheric visibility in urban beijing, China during the heating season. *Int. J. Environ. Res. Public Health* 15 (9), 1924. doi:10.3390/ijerph15091924

Liu, X., Sun, K., Qu, Y., Hu, M., Sun, Y., Zhang, F., et al. (2015). Secondary Formation of sulfate and nitrate during a haze episode in megacity beijing, China. *Aerosol Air Qual. Res.* 15 (6), 2246–2257. doi:10.4209/aaqr.2014.12.0321

Ma, J., Chu, B., Liu, J., Liu, Y., Zhang, H., and He, H. (2018). NOx promotion of SO_2 conversion to sulfate: An important mechanism for the occurrence of heavy haze during winter in Beijing. *Environ. Pollut.* 233, 662–669. doi:10.1016/j.envpol.2017.10.103

Pang, N. N., Gao, J., Che, F., Ma, T., Liu, S., Yang, Y., et al. (2020). Cause of $PM_{2.5}$ pollution during the 2016-2017 heating season in beijing, tianjin, and langfang, China. *J. Environ. Sci.* 95, 201–209. doi:10.1016/j.jes.2020.03.024

Rai, P., Furger, M., Slowik, J. G., Zhong, H., Tong, Y., Wang, L., et al. (2021). Characteristics and sources of hourly elements in PM_{10} and $PM_{2.5}$ during wintertime in Beijing. *Environ. Pollut.* 278, 116865. doi:10.1016/j.envpol.2021.116865

Ren, C., Huang, X., Wang, Z., Sun, P., Chi, X., Ma, Y., et al. (2021). Nonlinear response of nitrate to NOx reduction in China during the COVID-19 pandemic. *Atmos. Environ. X.* 264, 118715. doi:10.1016/j.atmosenv.2021.118715

Shao, J., Chen, Q., Wang, Y., Lu, X., He, P., Sun, Y., et al. (2019). Heterogeneous sulfate aerosol formation mechanisms during wintertime Chinese haze events: Air quality model assessment using observations of sulfate oxygen isotopes in beijing. *Atmos. Chem. Phys.* 19 (9), 6107–6123. doi:10.5194/acp-19-6107-2019

Shen, J., Tang, A., Liu, X., Kopsch, J., Fangmeier, A., Goulding, K., et al. (2011). Impacts of pollution controls on air quality in beijing during the 2008 olympic games. *J. Environ. Qual.* 40 (1), 37–45. doi:10.2134/jeq2010.0360

Su, J., Zhao, P., Ding, J., Du, X., and Dou, Y. (2021). Insights into measurements of water-soluble ions in PM2.5 and their gaseous precursors in Beijing. *J. Environ. Sci.* 102, 123–137. doi:10.1016/j.jes.2020.08.031

Sun, J., Liang, M., Shi, Z., Shen, F., Li, J., Huang, L., et al. (2019). Investigating the $PM_{2.5}$ mass concentration growth processes during 2013-2016 in Beijing and Shanghai. *Chemosphere* 221, 452–463. doi:10.1016/j.chemosphere.2018.12.200

Sun, Y., Wang, Z., Fu, P., Jiang, Q., Yang, T., Li, J., et al. (2013). The impact of relative humidity on aerosol composition and evolution processes during wintertime in Beijing, China. *Atmos. Environ. X.* 77, 927–934. doi:10.1016/j.atmosenv.2013.06.019

Wang, H., Lu, K., Tan, Z., Chen, X., Liu, Y., and Zhang, Y. (2022a). Formation mechanism and control strategy for particulate nitrate in China. *J. Environ. Sci.* doi:10.1016/j.jes.2022.09.019

Wang, J., Li, J., Ye, J., Zhao, J., Wu, Y., Hu, J., et al. (2020). Fast sulfate formation from oxidation of SO_2 by NO_2 and HONO observed in Beijing haze. *Nat. Commun.* 11 (1), 2844. doi:10.1038/s41467-020-16683-x

Wang, S., Wang, L., Fan, X., Wang, N., Ma, S., and Zhang, R. (2022b). Formation pathway of secondary inorganic aerosol and its influencing factors in Northern China: Comparison between urban and rural sites. *Sci. Total Environ.* 840, 156404. doi:10.1016/j.scitotenv.2022.156404

Wang, T., Liu, M., Liu, M., Song, Y., Xu, Z., Shang, F., et al. (2022d). Sulfate Formation apportionment during winter haze events in north China. *Environ. Sci. Technol.* 56 (12), 7771–7778. doi:10.1021/acs.est.2c02533

Wang, T., Liu, Y., Cheng, H., Wang, Z., Fu, H., Chen, J., et al. (2022c). Significant formation of sulfate aerosols contributed by the heterogeneous drivers of dust surface. *Atmos. Chem. Phys.* 22 (20), 13467–13493. doi:10.5194/acp-22-13467-2022

Wang, W., Liu, M., Wang, T., Song, Y., Zhou, L., Cao, J., et al. (2021). Sulfate formation is dominated by manganese-catalyzed oxidation of SO_2 on aerosol surfaces during haze events. *Nat. Commun.* 12 (1), 1993. doi:10.1038/s41467-021-22091-6

Wang, X., Wei, W., Cheng, S., Yao, S., Zhang, H., and Zhang, C. (2019a). Characteristics of $PM_{2.5}$ and SNA components and meteorological factors impact on air pollution through 2013–2017 in Beijing, China. *Atmos. Pollut. Res.* 10 (6), 1976–1984. doi:10.1016/j.apr.2019.09.004

Wang, Y., Wang, Q., Ye, J., Yan, M., Qin, Q., Prevot, A. S. H., et al. (2019b). A review of aerosol chemical composition and sources in representative regions of China during wintertime. *Atmosphere* 10 (5), 277. doi:10.3390/atmos10050277

Wang, Y., Yao, L., Wang, L., Liu, Z., Ji, D., Tang, G., et al. (2013). Mechanism for the formation of the January 2013 heavy haze pollution episode over central and eastern China. *Sci. China Earth Sci.* 57 (1), 14–25. doi:10.1007/s11430-013-4773-4

Wu, L., Sun, J., Zhang, X., Zhang, Y., Wang, Y., Zhong, J., et al. (2019). Aqueous-phase reactions occurred in the $PM_{2.5}$ cumulative explosive growth during the heavy pollution episode (HPE) in 2016 Beijing wintertime. *Tellus, Ser. B Chem. Phys. Meteorol.* 71 (1), 1–15. doi:10.1080/16000889.2019.1620079

Wu, L., Wang, Y., Li, L., and Zhang, G. (2020). Acidity and inorganic ion formation in PM2.5 based on continuous online observations in a South China megacity. *Atmos. Pollut. Res.* 11 (8), 1339–1350. doi:10.1016/j.apr.2020.05.003

Wu, L., Zhang, X., Sun, J., Wang, Y., Zhong, J., and Meng, Z. (2022). Intensified wintertime secondary inorganic aerosol formation during heavy haze pollution episodes (HPEs) in Beijing, China. *J. Environ. Sci.* 114, 503–513. doi:10.1016/j.jes.2022.01.008

Xie, X., Hu, J., Qin, M., Guo, S., Hu, M., Wang, H., et al. (2022). Modeling particulate nitrate in China: Current findings and future directions. *Environ. Int.* 166, 107369. doi:10.1016/j.envint.2022.107369

Xu, M., Liu, Z., Hu, B., Yan, G., Zou, J., Zhao, S., et al. (2022). Chemical characterization and source identification of $PM_{2.5}$ in Luoyang after the clean air actions. *J. Environ. Sci.* 115, 265–276. doi:10.1016/j.jes.2021.06.021

Xu, Q., Wang, S., Jiang, J., Bhattarai, N., Li, X., Chang, X., et al. (2019a). Nitrate dominates the chemical composition of $PM_{2.5}$ during haze event in

Beijing, China. *Sci. Total Environ.* 689, 1293–1303. doi:10.1016/j.scitotenv.2019.06.294

Xu, W., Liu, X., Liu, L., Dore, A. J., Tang, A., Lu, L., et al. (2019b). Impact of emission controls on air quality in Beijing during APEC 2014: Implications from water-soluble ions and carbonaceous aerosol in $PM_{2.5}$ and their precursors. *Atmos. Environ. X.* 210, 241–252. doi:10.1016/j.atmosenv.2019.04.050

Yang, J., Wang, S., Zhang, R., and Yin, S. (2022). Elevated particle acidity enhanced the sulfate formation during the COVID-19 pandemic in Zhengzhou, China. *Environ. Pollut.* 296, 118716. doi:10.1016/j.envpol.2021.118716

Yang, S., Ma, Y., Duan, F., He, K., Wang, L., Wei, Z., et al. (2018). Characteristics and formation of typical winter haze in Handan, one of the most polluted cities in China. *Sci. Total Environ.* 613-614, 1367–1375. doi:10.1016/j.scitotenv.2017.08.033

Ye, C., Lu, K., Song, H., Mu, Y., Chen, J., and Zhang, Y. (2022). A critical review of sulfate aerosol formation mechanisms during winter polluted periods. *J. Environ. Sci.* doi:10.1016/j.jes.2022.07.011

Yun, H., Wang, W., Wang, T., Xia, M., Yu, C., Wang, Z., et al. (2018). Nitrate formation from heterogeneous uptake of dinitrogen pentoxide during a severe winter haze in southern China. *Atmos. Chem. Phys.* 18 (23), 17515–17527. doi:10.5194/acp-18-17515-2018

Zhan, Y., Xie, M., Gao, D., Wang, T., Zhang, M., and An, F. (2021). Characterization and source analysis of water-soluble inorganic ionic species in $PM_{2.5}$ during a wintertime particle pollution episode in Nanjing, China. *Atmos. Res.* 262, 105769. doi:10.1016/j.atmosres.2021.105769

Zhang, R., Sun, X. S., Shi, A. J., Huang, Y. H., Yan, J., Nie, T., et al. (2018a). Secondary inorganic aerosols formation during haze episodes at an urban site in Beijing, China. *Atmos. Environ. X.* 177, 275–282. doi:10.1016/j.atmosenv.2017.12.031

Zhang, Y., Li, X., Nie, T., Qi, J., Chen, J., and Wu, Q. (2018b). Source apportionment of $PM_{2.5}$ pollution in the central six districts of Beijing, China. *J. Clean. Prod.* 174, 661–669. doi:10.1016/j.jclepro.2017.10.332

Zhao, L., Wang, L., Tan, J., Duan, J., Ma, X., Zhang, C., et al. (2019). Changes of chemical composition and source apportionment of $PM_{2.5}$ during 2013–2017 in urban Handan, China. *Atmos. Environ. X.* 206, 119–131. doi:10.1016/j.atmosenv.2019.02.034

Zhong, J., Zhang, X., Dong, Y., Wang, Y., Liu, C., Wang, J., et al. (2018a). Feedback effects of boundary-layer meteorological factors on cumulative explosive growth of $PM_{2.5}$ during winter heavy pollution episodes in Beijing from 2013 to 2016. *Atmos. Chem. Phys.* 18 (1), 247–258. doi:10.5194/acp-18-247-2018

Zhong, J., Zhang, X., Wang, Y., Liu, C., and Dong, Y. (2018b). Heavy aerosol pollution episodes in winter Beijing enhanced by radiative cooling effects of aerosols. *Atmos. Res.* 209, 59–64. doi:10.1016/j.atmosres.2018.03.011

Zhong, J., Zhang, X., Wang, Y., Sun, J., Zhang, Y., Wang, J., et al. (2017). Relative contributions of boundary-layer meteorological factors to the explosive growth of $PM_{2.5}$ during the red-alert heavy pollution episodes in Beijing in December 2016. *J. Meteorol. Res.* 31 (5), 809–819. doi:10.1007/s13351-017-7088-0